

The Size and Shape of Local Voids

Manolis Plionis¹ & Spyros Basilakos²

¹ Institute of Astronomy & Astrophysics, National Observatory of Athens, I.Metaxa & B.Pavlou, Palaia Penteli, 152 36, Athens, Greece

² Astrophysics Group, Imperial College London, Blackett Laboratory, Prince Consort Road, London SW7 2BW, UK

2 December 2024

ABSTRACT

We study the size and shape of low density regions in the local universe which we identify in the smoothed density field of the PSCz flux limited IRAS galaxy catalogue. After quantifying the systematic biases that enter in the detection of voids using our data set and method, we identify 14 voids within $80 h^{-1}$ Mpc and with volumes $\geq 10^3 h^{-3}$ Mpc and 8 voids within $130 h^{-1}$ Mpc and with volumes $\geq 8 \times 10^3 h^{-3}$ Mpc. We study the void size distribution and morphologies and find that there is roughly an equal number of prolate and oblate-like spheroidal voids. We compare the measured PSCz void shape and size distributions with those expected in six different CDM models and find that only the latter distribution can discriminate between models. The models preferred by the PSCz data are those with intermediate values of σ_8 ($\simeq 0.83$). **Keywords:** cosmology:theory - galaxies: general - large-scale structure of universe - Infrared: galaxies

1 INTRODUCTION

Many authors have claimed that low density regions (voids) are the most common features of the large scale structure of the universe owing to the fact that they occupy more than a half of its volume. Individual voids and their properties have been investigated by different authors (cf. Joëveer et al. 1978; Kirshner et al. 1981; Rood 1981 and references that he gives). Since their creation has been attributed to the effects of gravitational instability (cf. Zeldovich, Einasto & Shandarin 1982; Coles, Melott & Shandarin 1993; Peebles 2001 and references therein), the distribution of voids on large scales could provide important constraints on models of structure formation. From N-body simulations it has become evident that in the hierarchical structure formation scenario, matter collapses and forms high density objects, like clusters and superclusters, and enhance the underdense regions between them (cf. Melott et al. 1983). Therefore, if the above view is correct then the morphological and statistical properties of voids (size, shape) should depend on the initial power spectrum $P(k)$ and on the density parameter Ω_0 (cf. White 1979; Melott 1987; Einasto, Einasto & Gramann 1989; Regös & Geller 1991; Ryden & Melott 1996).

In order to study in an objective manner the distribution of voids and their physical properties it is necessary to develop objective void-finding algorithms and to apply them onto well controlled data. Such attempts were pioneered by Kauffmann & Fairall (1991), Kauffmann & Melott (1992) and more recently by El-Ad, Piran & da Costa (1996), El-Ad & Piran (1997) and

Stavrev (2000). El-Ad, Piran & da Costa (1997) applied their void-finding algorithm to the IRAS 1.2Jy galaxy catalogue and found, within $80 h^{-1}$ Mpc, 15 voids with an average diameter of $40 \pm 6 h^{-1}$ Mpc. Müller et al. (2001) have also studied the distribution of voids and their sizes using the large Las Campanas Redshift Survey and compared their properties with CDM simulations. They found that although the void-size distribution provides important information on the large-scale distribution of matter, galaxy biasing seems more important in defining voids than differences between the cosmological models.

In this paper we use the PSCz-IRAS redshift survey in order to measure the void size and shape distributions in the local universe and to investigate whether these distributions can be used as cosmological probes. The plan of the paper is the following: In section 2 we briefly describe the PSCz data. In section 3 we present the void identification and shape determination procedure, the systematic effects that affect the PSCz void detection and our results. We compare our PSCz results with the corresponding ones of six cosmological models in section 4 and finally in section 5 we draw our conclusions.

2 THE PSCZ GALAXY SAMPLE

In our analysis we use the recently completed IRAS flux-limited 60- μ m redshift survey (PSCz) which is described in Saunders et al. (2000). The PSCz catalogue contains ~ 15500 galaxies with flux $S_{lim} \geq 0.6$ Jy covering the $\sim 84\%$ of the sky.

In order to construct an unbiased continuous density field we have to take into account the well-known degradation of sampling as a function of distance due to the fact that the PSCz catalogue is a flux limited sample. This is done by weighting each galaxy by the inverse selection function, assuming that the unobserved galaxies are spatially correlated with the observed ones. Note that the selection function is defined as the fraction of the galaxy number density that is observed above the flux limit at some distance r . We estimate the selection function by using the functional form of the IRAS galaxy luminosity function of Saunders et al. (1990) with parameters: $L_* = 10^{8.45} h^2 L_\odot$, $\sigma = 0.711$, $\alpha = 1.09$ and $C = 0.0308$ (Rowan-Robinson et al. 2000).

In order to treat the 16% excluded sky (galactic plane, high cirrus emission areas and unobserved regions) we use the PSCz data reduction of Branchini et al. (1999), in which they followed the Yahil et al. (1991) method to fill the galactic plane region with synthetic objects that reproduce the mean density of galaxies in the regions residing nearby.

Finally, in this kind of analysis it is essential to transform redshifts to 3D distances in order to minimise the so called “Kaiser” effect. This effect can be understood by noting that the distribution of galaxies in redshift space is a distorted representation of that in real comoving space due to their peculiar velocities (Kaiser 1987). In this paper we use the 3D distances determined by the iterative algorithm of Branchini et al (1999) for $\beta = 0.5$ ^{*}, since their recent VELMOD analysis strongly suggest such a value (Branchini et al. 2001).

3 PSCZ VOIDS

3.1 Smoothing Procedure

For the purpose of this study we need to derive from the discrete distribution of PSCz galaxies a smooth continuous density field. This is realized by utilizing a Gaussian kernel on a N^3 grid and using two smoothing radii, namely $R_{\text{sm}} = 5 h^{-1} \text{ Mpc}$ and $10 h^{-1} \text{ Mpc}$, to probe essentially different void sizes. We extend our smoothing procedure out to r_{max} , where $r_{\text{max}} = 130$ and $170 h^{-1} \text{ Mpc}$ respectively for the two smoothing radii while the size of each cell is set equal to R_{sm} . Therefore we use a grid of size of 52^3 and 34^3 respectively. As we verified in Basilakos, Plionis & Rowan-Robinson (2001), the coupling between the selection function and the constant radius smoothing results in a distorted smoothed density distribution, especially at large distances. Gaussian spheres, centered on distant cells, overestimate the true density in regions where galaxies are detected (due to the heavy selection function weighting), while in underdense regions they underestimate the true density. In Basilakos et al. (2001) we developed a phenomenological approach to correct such biases and verified that our

^{*} $\beta = \Omega_0^{0.6}/b_{\text{IRAS}}$, with b_{IRAS} the IRAS bias factor. Our results remain qualitatively the same also for $\beta = 1$.

procedure is effective in recovering especially the high-density end of the probability density function (*pdf*). In the present study we use such a corrected density field and investigate possible systematic effects using a Monte-Carlo approach (see section 3.4).

3.2 Void Detection

In order to find our void candidates we select all grid-cells with $|b| \geq 10^\circ$ and with an overdensity under a chosen threshold and then join together those having common boundaries. Due to the fact that voids should be identified as low density regions, the threshold value of the overdensity (δ_{th}) could be defined directly from the probability density function as its 10%-ile value ($\delta_{\text{th}} = -0.68$ and -0.39 for the $R_{\text{sm}} = 5 h^{-1} \text{ Mpc}$ and $R_{\text{sm}} = 10 h^{-1} \text{ Mpc}$ respectively). Using higher values of δ_{th} we tend to connect voids and percolate underdense regions through the whole volume. Finally, we choose to analyse the above candidate voids for two different limiting distances, namely $r_{\text{lim}} \simeq 80 h^{-1} \text{ Mpc}$ for $R_{\text{sm}} = 5 h^{-1} \text{ Mpc}$, and $r_{\text{lim}} \simeq 130 h^{-1} \text{ Mpc}$ for $R_{\text{sm}} = 10 h^{-1} \text{ Mpc}$ respectively in order to avoid distance dependent systematic effects (see section 3.4 and figure 1).

3.3 Shape Statistics

Shapes are estimated for those “voids” that consist of 8 or more connected underdense cells, utilizing the moments of inertia (I_{ij}) method to fit the best triaxial ellipsoid to the data (cf. Carter & Metcalfe 1980; Plionis, Barrow & Frenk 1991; Basilakos et al. 2001). We diagonalize the inertia tensor

$$\det(I_{ij} - \lambda^2 M_3) = 0 \quad (M_3 \text{ is } 3 \times 3 \text{ unit matrix}), \quad (1)$$

obtaining the eigenvalues $\alpha_1, \alpha_2, \alpha_3$ (where α_1 is the semi-major axes) from which we define the shape of the configuration since, the eigenvalues are directly related to the three principal axes of the fitted ellipsoid. The volume of each void is then $V = \frac{4\pi}{3} \alpha_1 \alpha_2 \alpha_3$.

The shape statistic procedure, that we use, is based on a differential geometry approach, introduced by Sahni et al (1998) [for application to astronomical data see Basilakos et al. 2001]. Here we review only some basic concepts. A set of three shapefinders are defined having dimensions of length; $\mathcal{H}_1 = VS^{-1}$, $\mathcal{H}_2 = SC^{-1}$ and $\mathcal{H}_3 = C$, with S the surface area and C the integrated mean curvature. Then it is possible to define a set of two dimensional shapefinders K_1 and K_2 , as:

$$K_1 = \frac{\mathcal{H}_2 - \mathcal{H}_1}{\mathcal{H}_2 + \mathcal{H}_1} \quad (2)$$

and

$$K_2 = \frac{\mathcal{H}_3 - \mathcal{H}_2}{\mathcal{H}_3 + \mathcal{H}_2}, \quad (3)$$

normalized to give $\mathcal{H}_i = R$ ($K_{1,2} = 0$) for a sphere of radius R . Therefore, based on these shapefinders we can characterise the morphology of cosmic structures (underdense or overdense regions) according to the following categories: (i) oblate-like ellipsoids for $K_1/K_2 > 1$; (ii) prolate-like ellipsoids for $K_1/K_2 < 1$; (iii) triaxial

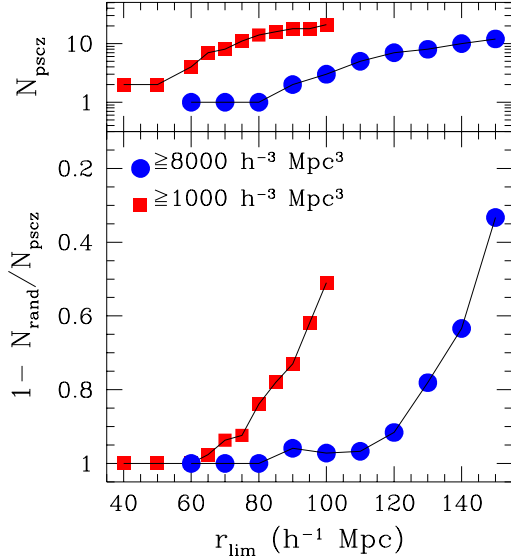


Figure 1. Statistical significance of our void detection procedure as a function of distance using either $R_{sm} = 5h^{-1}\text{Mpc}$ or $R_{sm} = 10h^{-1}\text{Mpc}$.

for $K_1/K_2 \simeq 1$ and (iv) spheres for $\alpha_1 \simeq \alpha_2 \simeq \alpha_3$ and thus $(K_1, K_2) \simeq (0, 0)$. For the quasi-spherical objects the ratio K_1/K_2 measures the deviation from pure sphericity.

3.4 Test for systematic errors

We run a large number of Monte-Carlo simulations in which we destroy the intrinsic PSCz galaxy clustering by randomising the angular coordinates of the galaxies while keeping their distances and therefore their selection function unchanged. On this intrinsically random galaxy distribution, utilizing the procedure described before, we identify the expected random voids, N_{rand} , which are due to our void-identification method itself. In figure 1 we plot for the different smoothing radii, the probability of detecting real voids in the PSCz data, defined as $\mathcal{P} = 1 - N_{\text{rand}}/N_{\text{PSCz}}$, as well as the number of real PSCz voids, N_{PSCz} . In the presence of negligible systematic biases in our method and data, the above selection process should result in $\mathcal{P} \simeq 1$, at all distances.

We find that the number of random voids increases with distance, a fact which should be attributed to the coupling of the PSCz selection function and the constant radius smoothing. Our phenomenological method of recovering the true density field (Basilakos et al. 2001) is multiplicative in nature and thus it is unable to correct the low and zero density cells. Therefore, the lower part of the *pdf* cannot be recovered efficiently. In particular we find that for $R_{sm} = 5h^{-1}\text{Mpc}$ smoothing radius (figure 1, squares), we have $\mathcal{P} > 0.8$ for detecting real voids within $r \leq 80^{-1}\text{Mpc}$ while for the $R_{sm} = 10h^{-1}\text{Mpc}$ smoothing radius (figure 1, circles), a similar probability is found within $r \leq 130^{-1}\text{Mpc}$. Note that for the largest voids in our sample this probability is much larger (>0.98).

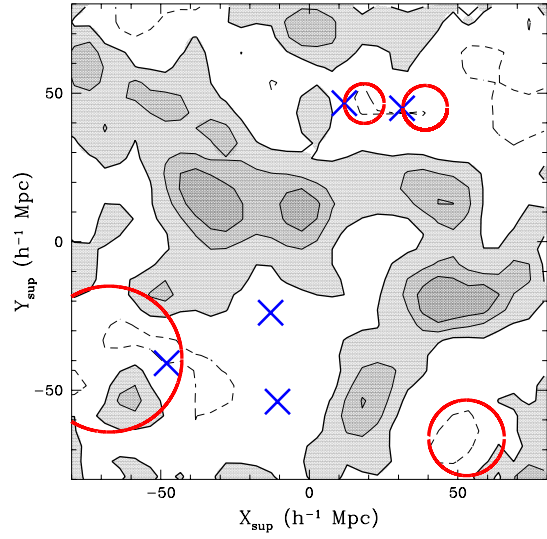


Figure 2. The smooth PSCz density field on the Supergalactic Plane out to $90 h^{-1}\text{Mpc}$. Large circles represent our detected voids (with sizes proportional to their volume) and crosses represent those of El-Ad et al. (1997) (with $-17 < Z_{sup} < 17 h^{-1}$).

3.5 The PSCz Void Cosmography

In figure 2 we plot the smoothed PSCz galaxy distribution on the supergalactic plane out to $90 h^{-1}\text{Mpc}$. The contour step is $\Delta\delta = 0.6$, starting from $\delta_{th} = -0.68$ while the $\delta = 0$ level appears as a thick continuous line. All major known clusters are present, like the Virgo cluster at $X_{sup} \simeq -5$, $Y_{sup} \simeq 5$; the Hydra-Centaurus at $X_{sup} \simeq 35$, $Y_{sup} \simeq 15$; the Perseus at $X_{sup} \simeq 50$, $Y_{sup} \simeq -20$ and the Coma at $X_{sup} \simeq 0$, $Y_{sup} \simeq 70$. We also plot the voids that we have detected as big circles while as crosses we mark the IRAS 1.2Jy voids found by El-Ad et al. (1997). We observe that our respective voids have almost identical positions. However, we do not detect two IRAS 1.2Jy voids, which in one case is due to a slight difference in the void Z_{sup} -position (our void No5 in table 1) and in the other it is probably due to our adopted overdensity threshold.

Details for those voids that consist of 8 or more cells are presented in table 1 and 2 for both smoothing radii; the different columns being self explanatory. Evidently 8 voids out of 14 are prolate-like ellipsoids and the rest oblate-like. While from table 2, we see that we have a slight excess of oblate-like voids, with one purely triaxial void ($K_1/K_2 \simeq 1$). Regarding extreme shaped voids, we have found, in the $R_{sm} = 5 h^{-1}\text{Mpc}$ field, two very prolate voids (see table 1: void 2 and 9), while in the $R_{sm} = 10 h^{-1}\text{Mpc}$ field, we again find two such prolate-like voids (see table 2: voids 6 and 8).

The median value of the semi-major void axes is $\sim 20 h^{-1}\text{Mpc}$ and $\sim 28 h^{-1}\text{Mpc}$ for $R_{sm} = 5 h^{-1}\text{Mpc}$ and $R_{sm} = 10 h^{-1}\text{Mpc}$ fields respectively, in good agreement with the results of El-Ad et al (1997).

Table 1. Detected voids in the $R_{sm} = 5 h^{-1}$ Mpc density field for $\delta \leq -0.69$ (corresponding to the 10%-ile) with $V \geq 10^3 h^{-3}$ Mpc 3 ($N_{\text{cell}} \geq 8$) and $r \leq 80 h^{-1}$ Mpc. The different columns are self-explanatory with column 3 being the distance of the void center and column 10 the void semi-major axis. The Local Void is No13 and the Sculptor Void is No4.

N	Volume ($10^3 h^{-3}$ Mpc 3)	d (h^{-1} Mpc)	X_{sup}	Y_{sup}	Z_{sup}	K_1	K_2	K_1/K_2	$\alpha_1 (h^{-1}\text{Mpc})$
1	8.6	77.4	14.8	-73.2	-20.6	0.040	0.060	0.67	20.7
2	2.4	72.6	-6.9	-58.4	42.5	0.073	0.205	0.35	19.9
3	12.6	78.5	69.6	-28.9	22.0	0.033	0.045	0.72	22.1
4	62.0	78.2	-67.4	-39.5	-4.8	0.039	0.042	0.94	36.8
5	3.8	33.9	-13.8	-24.9	-18.4	0.017	0.014	1.21	12.0
6	1.8	73.9	27.6	-28.2	62.5	0.070	0.041	1.70	10.9
7	2.2	38.6	-17.2	-16.7	30.3	0.021	0.031	0.67	11.6
8	8.9	70.0	13.6	34.1	-59.6	0.028	0.024	1.17	17.3
9	1.4	63.4	-42.9	33.3	-32.7	0.078	0.286	0.27	19.5
10	1.2	50.4	18.5	46.5	-6.0	0.102	0.063	1.61	11.1
11	1.8	60.6	39.0	45.1	-11.1	0.033	0.032	1.03	10.6
12	16.4	64.5	37.8	49.4	17.1	0.084	0.101	0.83	29.8
13	25.4	51.2	-10.6	30.3	39.9	0.079	0.042	1.86	26.6
14	1.9	71.6	-8.8	63.2	32.5	0.029	0.034	0.85	11.1

Table 2. Detected voids in the $R_{sm} = 10 h^{-1}$ Mpc density field for $\delta \leq -0.39$ (corresponding to the 10%-ile) with $V \geq 8 \times 10^3 h^{-3}$ Mpc 3 ($N_{\text{cell}} \geq 8$) and $r \leq 130 h^{-1}$ Mpc.

N	Volume ($10^4 h^{-3}$ Mpc 3)	d (h^{-1} Mpc)	X_{sup}	Y_{sup}	Z_{sup}	K_1	K_2	K_1/K_2	$\alpha_1 (h^{-1}\text{Mpc})$
1	2.5	129.6	-48.8	-115.3	33.5	0.063	0.050	1.27	28.1
2	63.8	117.3	37.8	-107.4	-27.9	0.077	0.048	1.60	81.7
3	1.2	58.5	-28.5	-50.9	5.0	0.067	0.059	1.14	23.0
4	0.9	103.6	72.8	-38.4	62.9	0.063	0.153	0.41	27.6
5	1.6	109.4	86.8	-23.3	-62.2	0.016	0.016	1.00	19.9
6	7.7	97.8	-80.3	-43.2	35.4	0.063	0.193	0.33	61.7
7	2.8	111.3	-6.4	72.9	-83.9	0.048	0.044	1.09	28.5
8	34.0	86.8	53.1	46.7	50.2	0.055	0.155	0.36	92.6

4 COMPARISON WITH COSMOLOGICAL MODELS

We use mock PSCz catalogues (Branchini et al. 1999) generated from six large cosmological N-body simulations of Cole et al. (1998), in order to investigate whether void properties (shapes and numbers) can discriminate between models. We consider six different cold dark matter models, which are: (1) a flat low-density CDM model ($\Lambda_{\text{CDM}1}$) with $\Omega_\Lambda = 0.7$ and shape parameter $\Gamma = 0.25$, (2) a flat model with $\Omega_\Lambda = 0.5$ and $\Gamma = 0.25$ ($\Lambda_{\text{CDM}2}$), (3) a critical density universe with $\Gamma = 0.25$ (τ_{CDM}) (4) an open model with $\Omega_o = 0.5$ (Ω_{CDM}) (5) a COBE normalized $\Omega_o = 1$, $\Gamma = 0.5$ model (C_{CDM}) and (6) the old ‘standard’ $\Omega_o = 1$ model with $\Gamma = 0.5$ and $\sigma_8 = 0.55$ (S_{CDM}). The first four are normalized by the observed cluster abundance at zero redshift; having fluctuation amplitude of $\sigma_8 = 0.55\Omega_o^{-0.6}$ (Eke, Cole, & Frenk 1996), while the fifth is COBE normalized with $\sigma_8 = 1.35$.

For each cosmological model we average results over 10 nearly independent mock PSCz catalogues extending out to a radius of $170 h^{-1}$ Mpc which were produced by Enzo Branchini (see Branchini et al. 1999). Good care was taken to center the catalogues to suitable LG-like observers (having similar to the observed Local Group velocity, shear and overdensity). We analyse the mock PSCz catalogues density fields (with $R_{sm} = 5 h^{-1}$ Mpc) in the same fashion as that of the observed PSCz catalogue. We find that the void shape distribution cannot discriminate among the different models, a result which

is similar with the shape-spectrum analysis of superclusters (see Basilakos et al 2001).

In figure 3 we plot the PSCz void-size frequency distribution in logarithmic bins and compare it with the outcome of all six models (hatched regions). We see that the models with similar value of σ_8 produce similar void-size distributions. We have verified this by using a Kolmogorov-Smirnov test on the unbinned distribution of void-sizes from all 10 realizations. Indeed, all pairs of model void-size distributions are excluded from being drawn from the same parent population at a high significance level ($> 99.9\%$), except for pairs that have similar values of σ_8 , ie., $\Lambda_{\text{CDM}1}$ - C_{CDM} , $\Lambda_{\text{CDM}2}$ - Ω_{CDM} and S_{CDM} - τ_{CDM} , which appear absolutely consistent among them.

Since in the model-data comparison we deal with only one realization of the Local Void distribution and since we have only 14 such voids, a rather small number for the K-S test to give reliable results (as we have verified using the K-S test with single model realizations), we quantify the differences between models and data by performing a standard binned χ^2 test, taking into account the scatter from the 10 different PSCz-like realizations. These probabilities are presented in table 3. Comparing the void-size distributions of the models among themselves we see that the χ^2 test is less sensitive to differences among the models with respect to the K-S test. With the exception of the C_{CDM} and τ_{CDM} models, which cannot be discriminated against, the other models follow the overall behaviour found by the K-S test when it was applied to the voids of all 10 realizations.

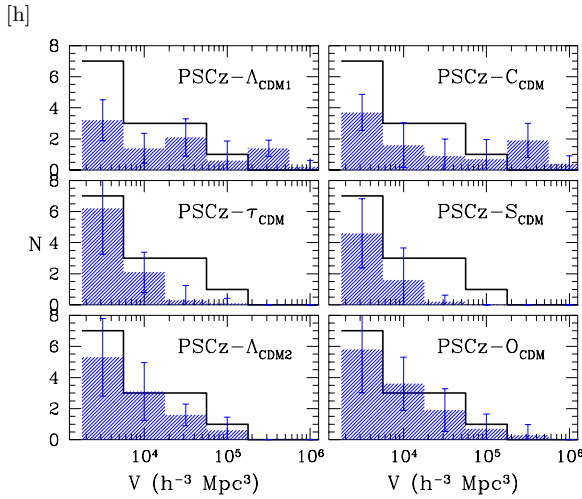


Figure 3. Void-size distribution comparison between the PSCz and look-alikes generated from 6 cosmological models. The model results are represented by the hatched regions and the errorbars represent the scatter among the 10 realizations of each model.

Table 3. χ^2 probability of the model and data void size distribution been drawn from the same parent distribution.

	Λ_{CDM1}	C_{CDM}	τ_{CDM}	S_{CDM}	Λ_{CDM2}	O_{CDM}
PSCz	0.002	0.006	0.001	0.000	0.195	0.870
Λ_{CDM1}	0.797	0.008	0.042	0.020	0.053	
C_{CDM}		0.114	0.428	0.221	0.302	
τ_{CDM}			0.906	0.166	0.408	
S_{CDM}				0.007	0.014	
Λ_{CDM2}					0.986	

Regarding the comparison between the PSCz and model voids, we see from both figure 3 and table 3 that the only models that fit the PSCz data, at a high significance level, are models with $\sigma_8 = 0.83$; ie., the Λ_{CDM2} and O_{CDM} , confirming the visual impression. Equivalent results are found by comparing the largest or most extremely shaped void of each realization with that of the PSCz data. This is not to say that an $\Omega_0 = 0.5$ should be preferred but rather that a $\sigma_8 \simeq 0.83$ CDM model is consistent with the data (similar results are found from the whole *pdf* study; Plionis & Basilakos 2001).

5 CONCLUSIONS

We have studied the properties of voids detected in the smoothed PSCz galaxy density field as connected regions under some overdensity threshold. We have investigated the biases that enter in the detection of voids using our procedure and the PSCz smoothed density field. We reliably detect 14 voids within $80 h^{-1}$ Mpc, in the $R_{sm} = 5 h^{-1}$ Mpc smoothed field, having a median semi-major axis of $\sim 20 h^{-1}$ Mpc and 8 voids in the relatively more distant Universe ($r \leq 130 h^{-1}$ Mpc) for the $R_{sm} = 10 h^{-1}$ Mpc smoothed field, having a me-

dian semi-major axis $\sim 28 h^{-1}$ Mpc. Finally, we have compared our PSCz void-size distribution with the corresponding ones generated from six cosmological models and we find that the CDM models that best reproduce the PSCz results are those with $\sigma_8 \simeq 0.83$.

ACKNOWLEDGMENTS

S.Basilakos has benefited from discussions with P.Coles. M.Plionis acknowledges the hospitality of the Astrophysics Group of Imperial College. We both thank E.Branchini for providing us with his reconstructed PSCz galaxy distribution and the PSCz look-alikes.

REFERENCES

Basilakos, S., Plionis, M., Rowan-Robinson, M., 2001, MNRAS, 323, 47
 Branchini, E., et al., 1999, MNRAS, 308, 1
 Branchini, E., Freudling, W., Da Costa, L.N., Frenk, C.S., Giovanelli, R., Haynes, M.P., Salzer, J.J., Wegner, G., Zehavi, I., 2001, MNRAS, *in press*
 Carter, D. & Metcalfe, J., 1980, MNRAS, 191, 325
 Cole, S., Hatton, S., Weinberg, D. H., Frenk, C. S., 1998, MNRAS, 300, 945
 Coles, P., Melott, A. L., Shandarin, S. F., 1993, MNRAS, 260, 765
 Einasto, J., Einasto, M., Gramann, M., 1989, MNRAS, 238, 155
 Eke, V., Cole, S., Frenk, C. S., 1996, MNRAS, 282, 263
 El-Ad, H., & Piran, T., 1997, ApJ, 491, 421
 El-Ad, H., Piran, T., da Costa, L. N., 1997, MNRAS, 287, 790
 El-Ad, H., Piran, T., da Costa, L. N., 1996, ApJ, 462, L13
 Jöeveer, M., Einasto, J., Tago, E., 1978, MNRAS, 185, 35
 Kauffmann, G., Fairall, A.P., 1991, MNRAS, 248, 313
 Kauffmann, G., Melott, A.L., 1992, ApJ, 393, 415
 Kirshner, R.P., Oemler A., Schechter, P.L., Shectman, S.A., 1981, ApJ, 248, L57
 Kaiser, N., 1987, ApJ, 284, L9 A&A, 301, 329
 Melott, A. L., Einasto, J., Saar, E., Suisalu, I., Klypin, A. A., Shandarin, S. F., 1983, PhRvL, 51, 935
 Melott, A. L., 1987, MNRAS, 228, 1001
 Melott, A. L., &, Shandarin, S. F., 1993, ApJ, 410, 469
 Müller, V., Arbabi-Bidgoli, S., Einasto, J., Tucker, D., 2000, MNRAS, 318, 280
 Peebles, P.J.E., 2001, ApJ, *in press*
 Plionis, M., Barrow J.D., Frenk, C.S., 1991, MNRAS, 249, 662
 Plionis, M., & Basilakos, S., 2001, MNRAS, submitted
 Regös, E., & Geller, M., 1991, ApJ, 377, 14
 Rood, H. J., 1981, RPPh, 44, 1077
 Rowan-Robinson, M., et al., 2000, MNRAS, 314, 37
 Ryden, B. S., & Melott, A. L., 1996, ApJ, 470, 160
 Sahni, V., Sathyapakash, B. S., Shandarin, S., 1998a, ApJ, 495, L5
 Saunders, W., Rowan-Robinson, M., Lawrence, A., Efstathiou, G., Kaizer, N., Ellis, R. S., Frenk, C. S., 1990, MNRAS, 242, 318
 Stavrev, K.Y., 2000, A&AS, 144, 323
 Saunders, W., et al., 2000, MNRAS, 317, 55
 White, S.D.M., 1979, MNRAS, 186, 145
 Yahil A., Strauss M., Davis M., Huchra J.P., 1991, ApJ, 372, 380

Zeldovich, Ya. B., Einasto, J., Shandarin, S., 1982, Nature, 300, 407